DIRAC-Note 2008-11
24 October 2008

Preshower Detector alignment

M.Pentia, S.Constantinescu, T.Ponta
National Institute for Physics and Nuclear Engineering, Bucharest, P.O.Box MG-6, RO-76900, ROMANIA.

Abstract

The Preshower Detector (PSh) data were analyzed and presented as one or two parameter distributions. They were fitted and described conveniently to be used in the DIRAC experimental data processing. The analysis was done for seven DIRAC run periodes during autumn 1999 and autumn 2001[a]

[a]Some discussions with the DIRAC collaborators is absolutely necessary to continue and to use the results in offline data anlysis

Contents

1 PSh detector characteristics

The main tasks of the PSh detector for DIRAC experiment [1] are to supply:

- amplitude signal for pion/electron separation
- time signal for zero level and one level triggers
- position information for particle track reconstruction by DNA

The PSh detector consists of 16 detector elements [3] (see Fig. 1). They are placed symmetrically along the two arms of the DIRAC setup, with 8 detector elements per arm.

The PSh aperture is 2800 $mm \times 750$ mm per arm. Each detector element (slab) consists of Pb converter and scintillation slab. The Pb converter thickness is 10 mm for low energy part (elements No.1,2,9,10) and 25 mm for high energy part (elements No.3,4,5,6,7,8, 11,12,13,14,15,16).

The plastic scintillator sheets (BC 408) were cut into rectangular slabs of sizes $350 \times 750 \times 10$ mm^3.

The EMI 9954-B 12-stage photomultiplier, 2 inch diameter, has been used for readout scintillator light signals, for each slab.

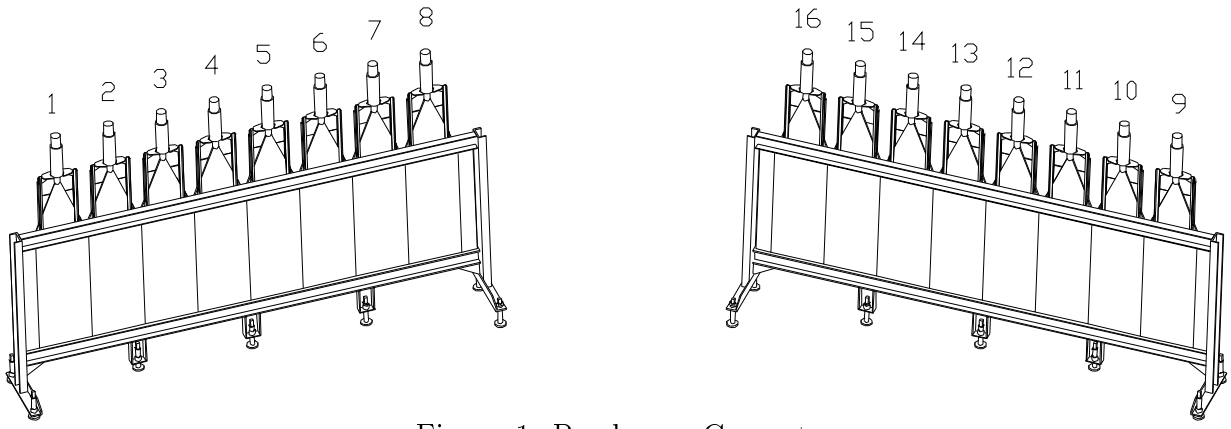

Figure 1: Preshower Geometry

The PSh detector elements (slabs) differ in some measure and induce inhomogeneities both in the individual and the global detector response. The effects can be observed in the PSh amplitude spectra or in coordinate and momentum distributions of the particles incident on PSh detector.

Typical raw data for ADC spectrum collected with T_{ee} trigger is shown in Fig. 2. In Fig. 3 the same data are corrected for *on-line suppression* and *pedestal position*, according to the relation

$$A = \text{ADC(measured)} + \text{online suppression - pedestal} \quad (1)$$

The *online suppression* and *pedestal position* data are presented in Table 1 and Table 2 for different Run periodes.

Table 1.

The *online suppression* values for each PSh slab, used in different DIRAC runs.

Run interval	1	2	3	4	5	6	7	8	9	10	11	12	13	14	15	16
100 - 795	45	50	46	47	48	46	51	48	50	39	44	57	45	42	47	42
796 - 1891	55	53	57	58	58	56	62	58	60	53	58	65	59	57	58	55
1892 -...	50	53	53	49	50	50	55	48	52	52	51	48	53	49	52	45

Table 2.

The *pedestal position* values for each PSh slab, used in different DIRAC runs.

Run interval	1	2	3	4	5	6	7	8	9	10	11	12	13	14	15	16
100 - 4072	39	44	42	41	41	38	47	41	44	37	42	48	43	39	46	42
4073-...	39	45	42	41	39	37	44	38	39	38	36	35	39	36	43	33

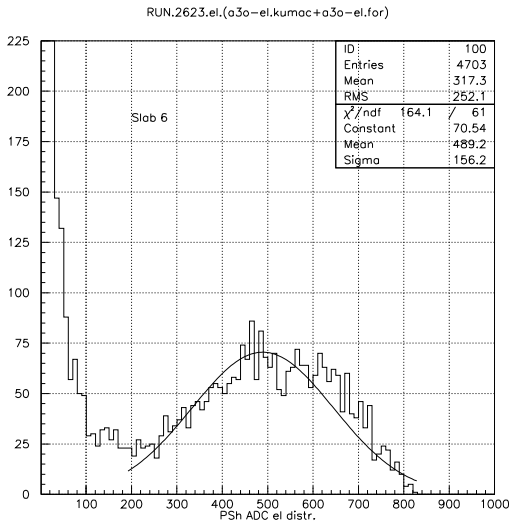

Figure 2: Raw PSh Slab 6 ADC data, collected in Run 2623 with T_{ee} trigger and $adc > 0.5$ condition. The electron distribution is fitted with a Gaussian function.

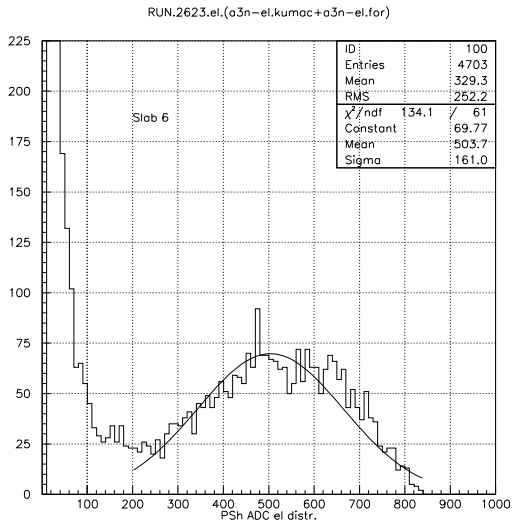

Figure 3: The PSh ADC data as in Fig.2, corrected for online suppression and pedestal position, according to Eq.(1). The electron distribution is fitted with a Gaussian function.

2 PSh slab inhomogeneities

Each scintillator slab placed behind the *Pb* converter provides the shower sampling. All low energy electrons and photons of the electromagnetic shower, produced by a relativistic electron, interact with the scintillator material and produce a large amplitude signal, proportional to the total *absorbed energy*. Therefore, the corrected amplitude (ADC) spectrum shows a broad distribution centered around a high amplitude mean value for electrons (Fig. 4).

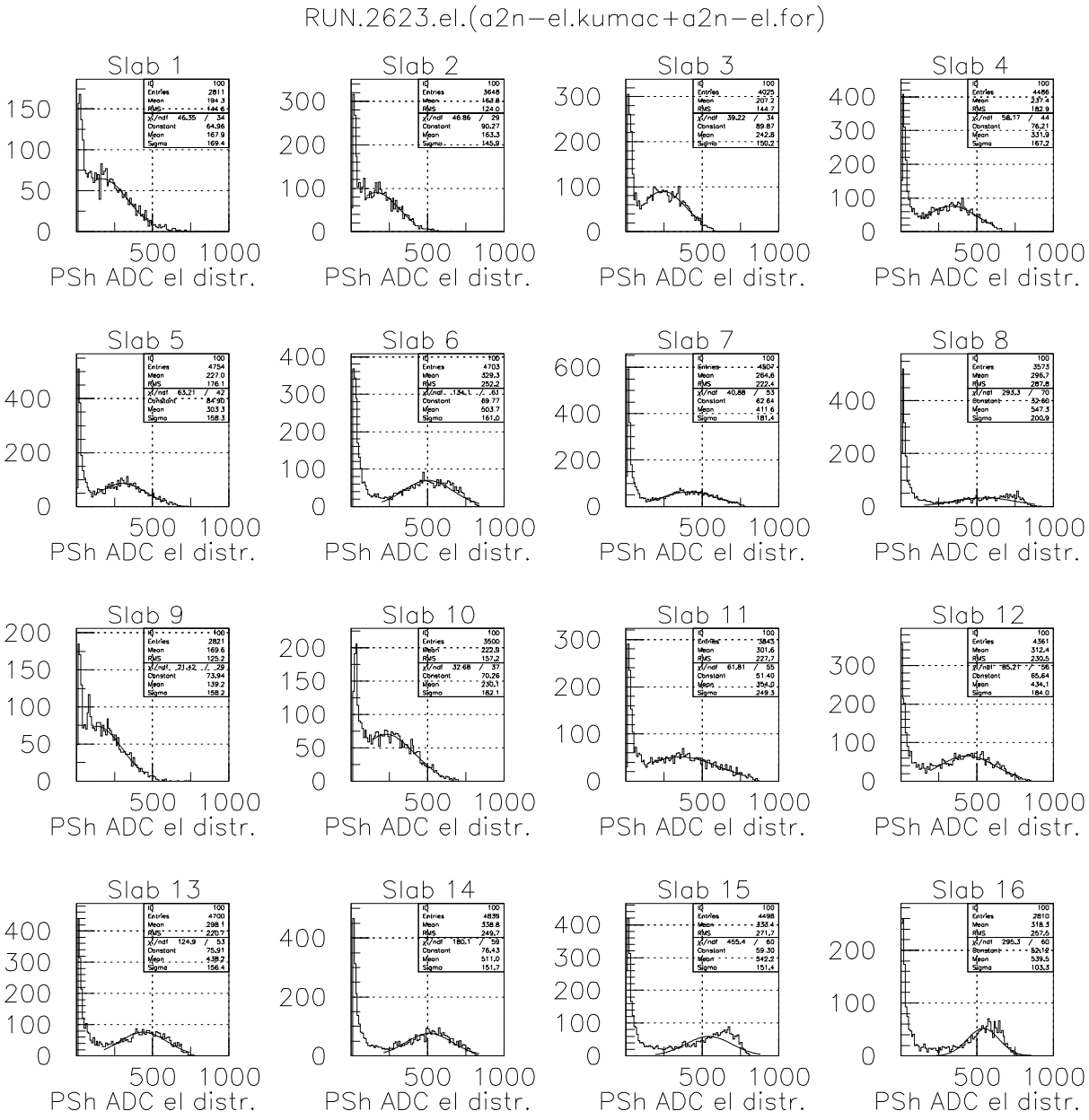

Figure 4: **Electron** amplitude distribution for individual PSh slabs collected in Run 2623 with T_{ee} trigger and $adc > 0.5$ condition, corrected according to Eq.(1).

On the other hand, the signal produced by a high energy pion has a low amplitude, because it losses energy mainly by direct ionization as *mip*'s. The amplitude spectrum shows a sharp peak around a low mean value (Fig. 5), and a higher amplitude tail due to the shower produced by some pions. The tail contribution increases with the pion energy (see Fig. 9).

The electron spectra were taken with T_{ee} trigger and the pion amplitude spectra were taken using $T_{\pi\pi copl}$ trigger, to separate $1+1$ *good pair events*.

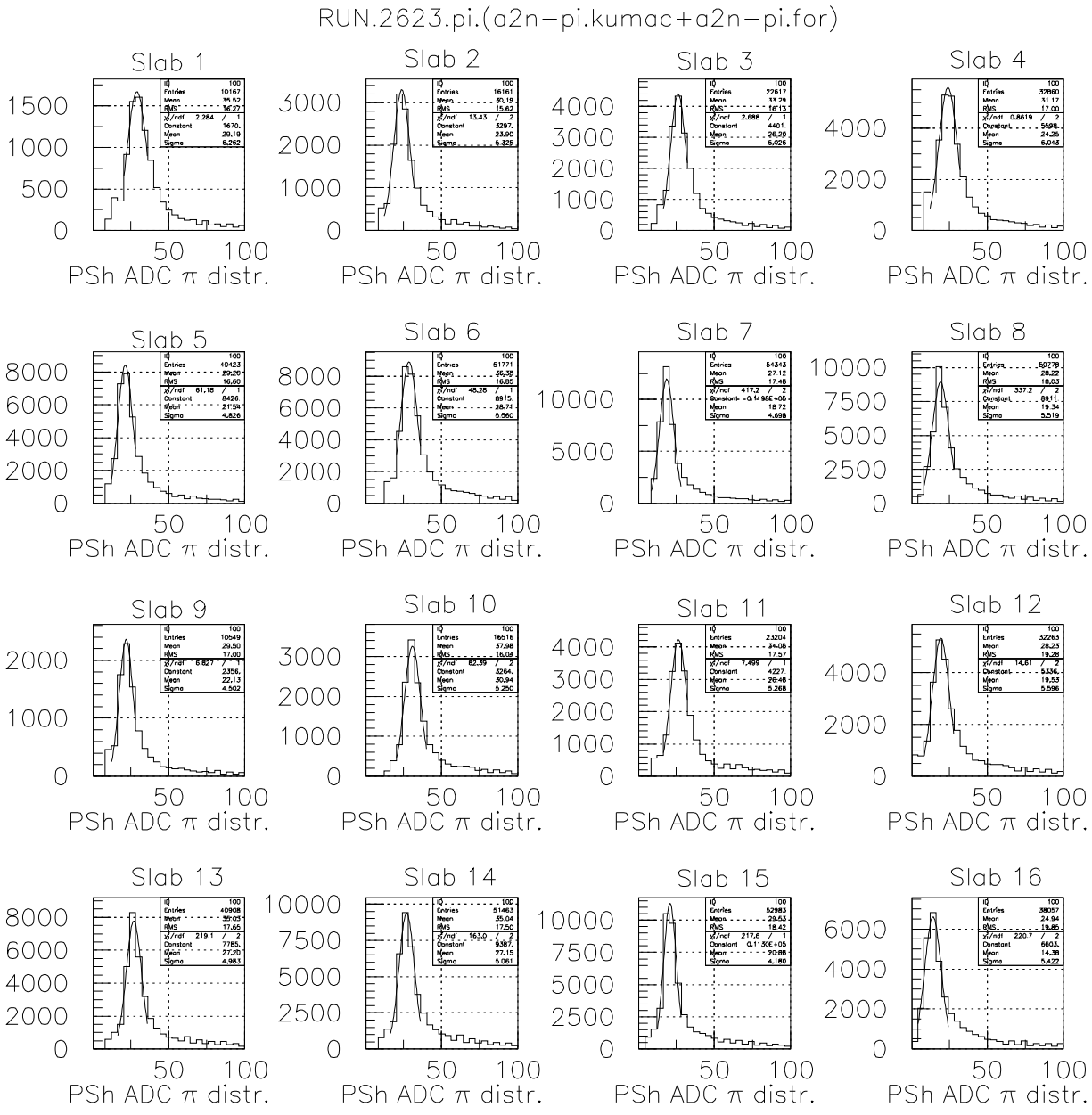

Figure 5: **Pion** amplitude distribution for individual PSh slabs collected in Run 2623 with $T_{\pi\pi copl}$ trigger and $adc > 0.5$ condition, corrected according to Eq.(1).

2.1 Electron amplitude - slab distributions

Figure 4 illustrates the **electron** corrected by Eq.(1) amplitude distribution for individual PSh slabs. They are momentum dependent and consequently the electron peak position differs from one slab to another (Fig. 6). The linear fit of these data:

$$Peak(channel) = a_0 + a_1 * Slab \tag{2}$$

gives the fit parameters a_0 and a_1, presented in **Table 3** for different DIRAC run periodes.

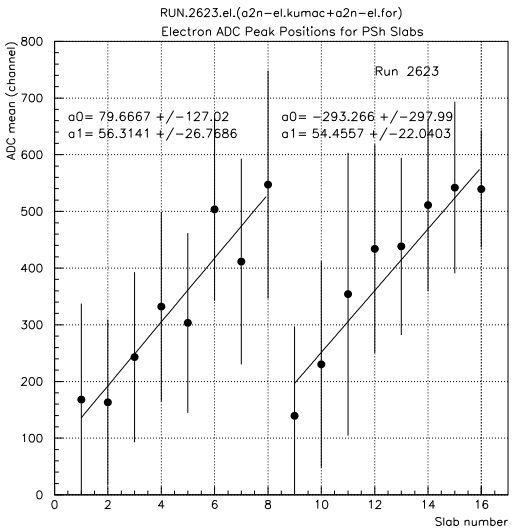

Figure 6: ADC mean value of the **electron** peak distribution (Gauss fit) as in Fig.4, for PSh slabs

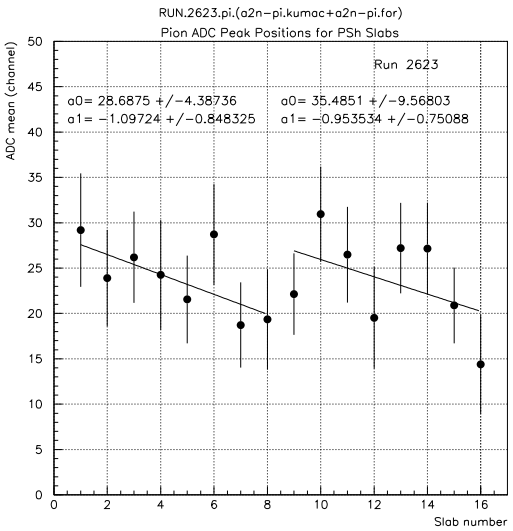

Figure 7: ADC mean value of the **pion** peak distribution (Gauss fit) as in Fig.5, for PSh slabs

Table 3.
Linear fit parameters of Eq.(2) for slab dependence of the **electron** peak position (Fig. 6).

Run (Season Year)	Target	Left arm		Right arm	
		a_0 (chan)	a_1 (ch/slab)	a_0 (chan)	a_1 (ch/slab)
1454 (Autumn 1999)	Pt	212.97	62.99	-159.01	54.36
2061 (Summer 2000)	Ni	74.36	62.64	-349.65	58.59
2623 (Autumn 2000)	Ti	79.67	56.31	-293.27	54.46
2844 (Autumn 2000)	Ti	69.16	62.85	-212.19	47.40
3180 (Spring 2001)	Ti	78.07	71.10	-196.88	54.91
3665 (Summer 2001)	Ni	32.73	68.74	-352.67	58.53
4255 (Autumn 2001)	Ni	39.11	71.02	-426.12	63.50

If we take the mean value of the amplitude, across the whole electron spectrum, the slab dependence (see Fig. 8) can be approximated again by a straight line:

$$Mean(channel) = a_0 + a_1 * Slab \tag{3}$$

In the same figure are plotted also the mean values of the amplitude/momentum ratio, for individual slabs.

The linear fit parameters of Eq.(3) for electron spectra are given in **Table 4**, for different DIRAC periode runs.

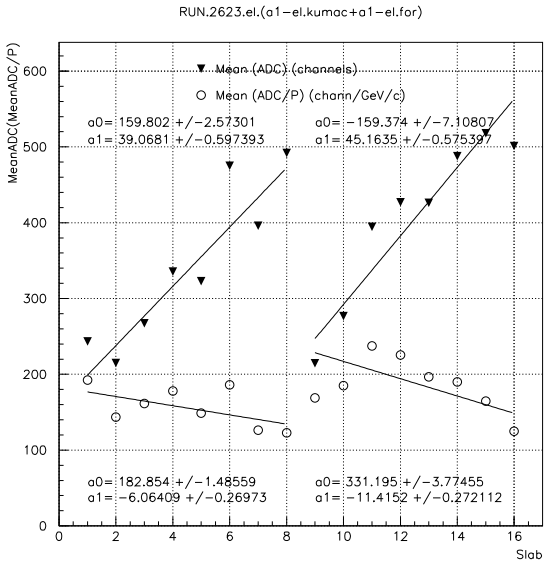

Figure 8: Overall ADC mean value of the **electron** distribution integrated on the slab

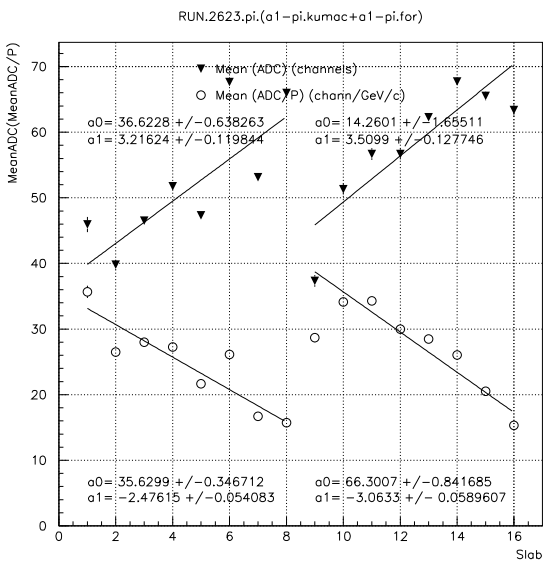

Figure 9: Overall ADC mean value of the **pion** distribution integrated on the slab

Table 4.

Linear fit parameters of Eq.(3) for slab dependence of the **electron** mean ADC and mean (ADC/p) (Fig. 8).

Run (Season Year)	Target	Mean ADC				Mean (ADC/p)			
		Left arm		Right arm		Left arm		Right arm	
		a_0 (chan)	a_1 (ch/sl)	a_0 (chan)	a_1 (ch/sl)	a_0 (chan)	a_1 (ch/sl)	a_0 (chan)	a_1 (ch/sl)
1454 (Autumn 1999)	Pt	270.95	46.57	-266.70	62.91	290.62	-14.07	337.74	-7.67
2061 (Summer 2000)	Ni	145.25	46.11	-235.69	50.89	179.86	-4.06	279.94	-7.76
2623 (Autumn 2000)	Ti	159.80	39.07	-159.37	45.16	182.85	-6.06	331.20	-11.42
2844 (Autumn 2000)	Ti	169.83	40.05	-145.83	43.84	195.16	-7.20	334.19	-11.83
3180 (Spring 2001)	Ti	182.44	43.95	-140.14	47.02	202.97	-5.54	368.49	-12.72
3665 (Summer 2001)	Ni	134.38	44.11	-216.75	48.74	163.44	-2.27	278.79	-7.87
4255 (Autumn 2001)	Ni	98.32	45.16	-333.63	53.58	134.27	0.60	164.83	-1.24

2.2 Pion amplitude - slab distributions

Figure 5 illustrates the pion ADC distribution for individual PSh slabs.

The pion peak distribution is practically momentum independent (Fig. 7).

If we take the mean value of the amplitude, across the whole spectrum on individual slabs, the pion dependence (Fig. 9) is quite similar to the electron one (Fig. 8).

The linear fit parameters of Eq.(3) for pion spectra are given in **Table 5**, for different DIRAC run periodes.

Table 5.
Linear fit parameters of Eq.(3) for slab dependence of the **pion** mean ADC and mean (ADC/p) (Fig. 9).

Run (Season Year)	Target	Mean ADC				Mean (ADC/p)			
		Left arm		Right arm		Left arm		Right arm	
		a_0 (chan)	a_1 (ch/sl)	a_0 (chan)	a_1 (ch/sl)	a_0 (chan)	a_1 (ch/sl)	a_0 (chan)	a_1 (ch/sl)
1454 (Autumn 1999)	Pt	-	-	-	-	-	-	-	-
2061 (Summer 2000)	Ni	34.85	4.10	3.85	4.26	35.76	-2.30	59.85	-2.61
2623 (Autumn 2000)	Ti	36.62	3.22	14.26	3.51	35.63	-2.48	66.30	-3.06
2844 (Autumn 2000)	Ti	39.54	2.78	23.96	2.68	37.28	-2.72	69.91	-3.35
3180 (Spring 2001)	Ti	31.57	5.78	8.22	4.47	33.60	-1.53	63.33	-2.63
3665 (Summer 2001)	Ni	31.28	4.13	5.20	3.90	30.99	-1.63	53.01	-2.17
4255 (Autumn 2001)	Ni	77.82	10.88	18.81	8.57	80.87	-4.51	128.81	-5.43

3 Impact position dependence

3.1 Electron amplitude - x and y correlations

The electron signal of the PSh detector is created mainly by shower particles. In Fig. 10 is shown the mean electron amplitude dependence versus x and y coordinates of the PSh detector, as profile plots. The inhomogeneities are evident. Also the interspaces existing between adjacent slabs can be seen. They are due to shower transversal development, leading to a partial detection of the shower particles by one slab, and consequently generating a lower amplitude.

There is also a small deep in the middle of the slabs No.3-8, 11-16. Here, the electron shower is larger (converter thickness is larger) and the light transmission is affected by the scintillator geometry. This effect has been studied, and the results are presented later, in Fig. 12.

The general trend of amplitude variation along x coordinate reflects the shower development as a function of the electron energy. The x-coordinate versus electron momentum correlation is presented in Fig. 16. The mean electron amplitude stands higher as the energy increases. The linear fit of this dependence

$$Mean(channel) = a_0 + a_1 * x(cm) \tag{4}$$

can be used to test the time stability of the PSh detector. In the **Table 6** are presented the linear fit parameters of Eq.(4) for different DIRAC run periodes.

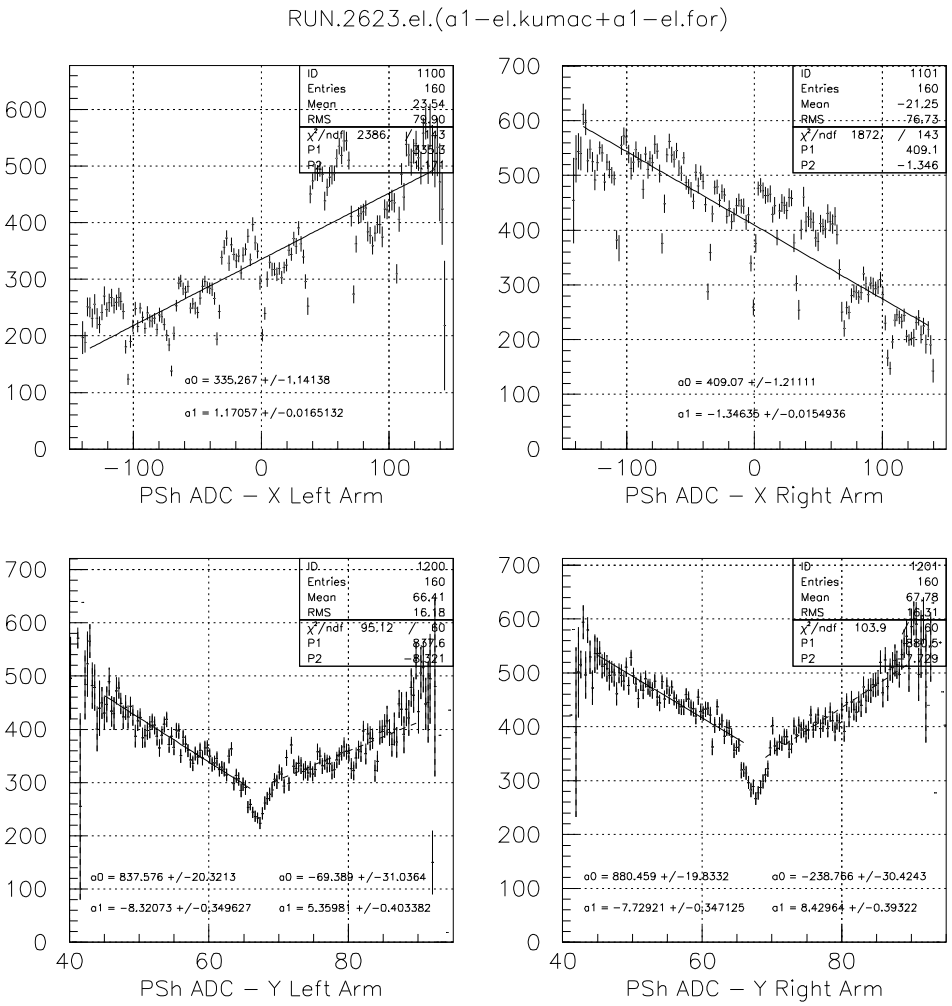

Figure 10: **Electron** amplitude (ADC channel) distribution versus x and y coordinate (cm)

Table 6.
Linear fit parameters of Eq.(4) for x coordinate dependence of the **electron** mean amplitude (Fig. 10 up)

Run (Season Year)	Target	Left arm		Right arm	
		a_0 (chan)	a_1 (ch/cm)	a_0 (chan)	a_1 (ch/cm)
1454 (Autumn 1999)	Pt	483.98	1.38	527.84	-1.92
2061 (Summer 2000)	Ni	352.21	1.34	402.96	-1.51
2623 (Autumn 2000)	Ti	335.27	1.17	409.07	-1.35
2844 (Autumn 2000)	Ti	350.43	1.18	404.64	-1.29
3180 (Spring 2001)	Ti	381.28	1.31	452.21	-1.41
3665 (Summer 2001)	Ni	332.50	1.29	395.59	-1.45
4255 (Autumn 2001)	Ni	302.05	1.35	337.63	-1.59

The y dependence for the electron amplitude is shown in the lower part of the Fig. 10. Here are evident two features:
1. A sharp energy degradation (lower amplitude) of the shower particles in the central part of the detector, due to previous electron interaction with the material before the PSh detector (aluminium table for Cherenkov PMT). See later the simulation results with Al (Fig. 13) and without Al (Fig. 14).
2. A small amplitude decrease, begining from the upper and lower boundaries to the center of the PSh detector. The linear description of these variations along the y coordinate, can be expressed as:

$$Mean(channel) = a_0 + a_1 * y(cm) \tag{5}$$

separately for the two vertical halves of the PSh detector (see Fig. 10 down). In the **Table 7** are presented the linear fit parameters for different DIRAC run periodes. In the pion case there is no any y dependence (Fig. 15 down). The electron amplitude decrease toward the scintillator center, along the y axis, is not a light transmission problem. It is given by the DIRAC setup configuration, as can be seen from the simulation studies (Fig. 13).

Table 7.
Linear fit parameters of the Eq.(5) for y dependence of the **electron** mean amplitude (Fig. 10 down)

Run (Season Year)	Target	Left arm				Right arm			
		lower half		upper half		lower half		upper half	
		a_0 (chan)	a_1 (ch/cm)	a_0 (chan)	a_1 (ch/cm)	a_0 (chan)	a_1 (ch/cm)	a_0 (chan)	a_1 (ch/cm)
1454 (Autumn 1999)	Pt	1027.94	-9.24	-69.76	7.20	1141.91	-10.47	-265.07	9.98
2061 (Summer 2000)	Ni	889.13	-8.93	-161.08	6.75	922.55	-8.54	-249.33	8.36
2623 (Autumn 2000)	Ti	837.58	-8.32	-69.39	5.36	880.46	-7.73	-238.77	8.43
2844 (Autumn 2000)	Ti	872.29	-8.66	-135.90	6.34	801.42	-6.40	-228.17	8.30
3180 (Spring 2001)	Ti	916.60	-8.95	-140.18	6.87	860.71	-6.59	-227.98	8.88
3665 (Summer 2001)	Ni	881.73	-9.10	-137.83	6.13	894.19	-8.25	-254.16	8.33
4255 (Autumn 2001)	Ni	806.83	-8.40	-171.50	6.25	885.90	-9.08	-311.56	8.34

3.1.1 Light transmission effects in the PSh scintillator slab

The experimental ADC versus x distribution for some of the slabs, (No: 3-8 and 11-16), present a valey in the slab mid (see Fig. 10). These are the slabs with thicker Pb converter (2.5 cm), which produces more intensive shower development. We tried to explain this feature. By light transmission simulation study in the scintillator slab, we sought for the x and y dependence of the light output yield.

The PSh scintillator slab characteristics, used in the simulation, are: dimensions: 350 $\times$ 750 $\times$ 10 mm^3; scintillator type: BICRON (BC-408), with light attenuation length: 210 cm. The wrapping material: Tyvek paper, not a polished surface. As a result, the light is diffused reflected, with a reflection efficiency about 60 %. The output directions are randomly distributed within $\pm 6^\circ$, around the symmetric reflection. The (x, y) light source points have been considered uniform distributed within the slab (see Fig. 11). The results, present the light output yield, at the PMT level, versus x and y slab coordinates (see Fig. 12). This can explain the qualitative behavior of the mean amplitude distribution versus x and y coordinate source points. Here is present a lower yield in the slab mid x distribution (Fig. 12.a) and also a lower yield at the slab far end on y, relative to PMT (Fig. 12.b).

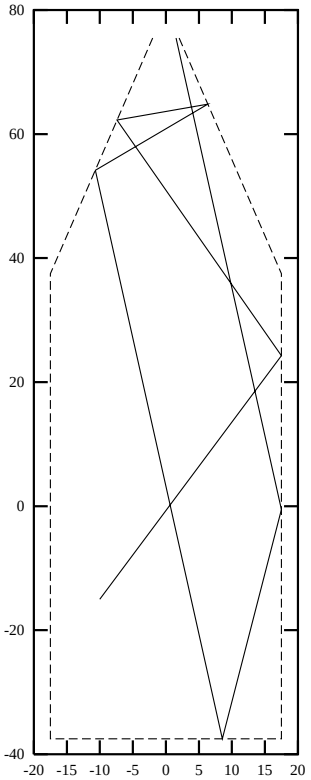

Figure 11: Simulated track light in the scintillator slab in $x - y$ plane.

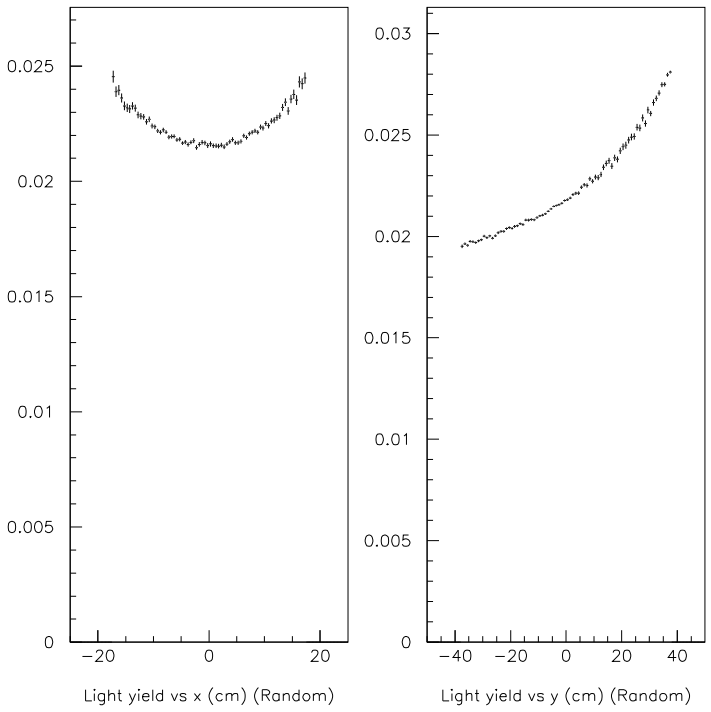

Figure 12: Simulated light output yield distributions to the PMT level, versus x and y source point coordinates within PSh scintillator slab.

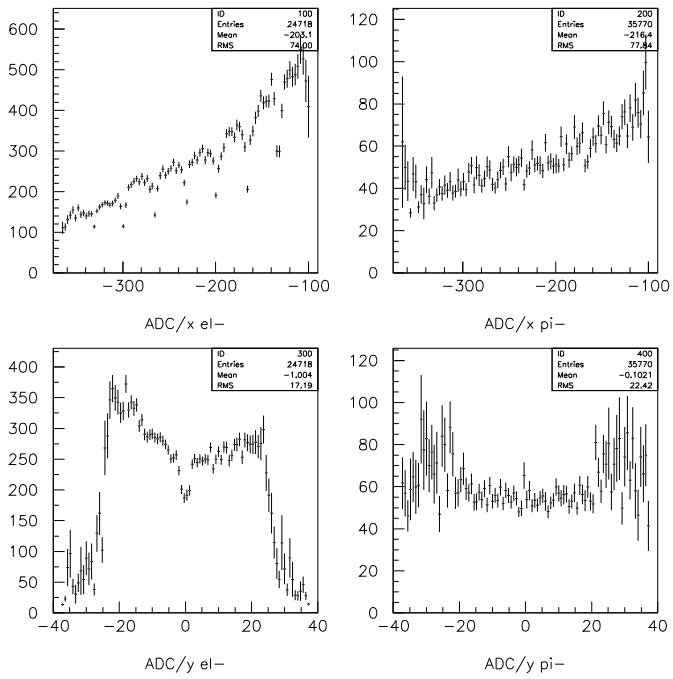

Figure 13: Simulated amplitude dependence on x and y coordinate hit of the PSh right arm (with *Al* table in the Cherenkov detector)

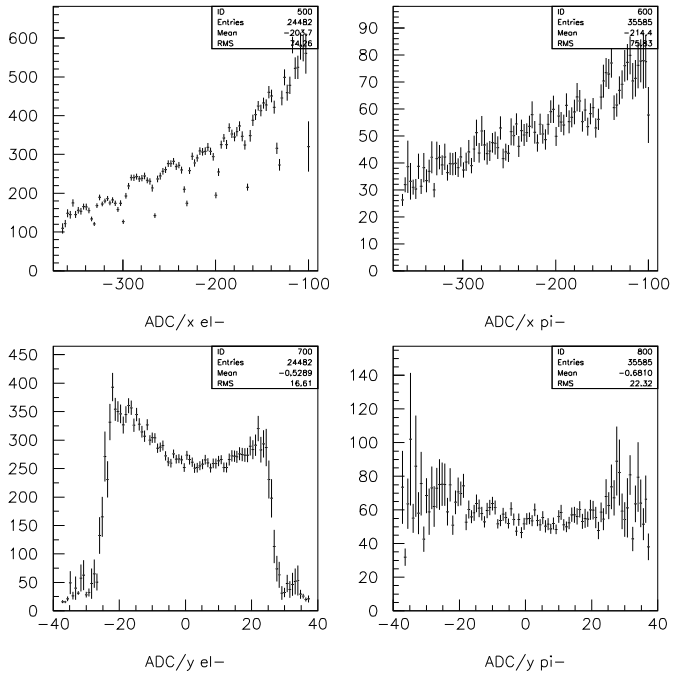

Figure 14: Simulated amplitude dependence on x and y coordinate hit of the PSh right arm (without *Al* table in the Cherenkov detector)

3.2 Pion amplitude - x and y correlations

The pion signal of the PSh detector is created mainly by direct ionisation. In Fig. 15 is shown the pion mean amplitude dependence versus x and y coordinates of the PSh detector, as profile plots. The same inhomogeneities along with x axis can be observed. Nevertheless, the interspaces between adjacent slabs can not be seen more. For most of the pions they are detected by directly interaction with the scintilator slab and produce the m.i.p. peak (Fig. 5). On the other hand, some of them can develop shower, as their momentum increases. This can be seen in Fig. 15 as a small increase of the mean amplitude with x.
The mean pion amplitude stands higher as its energy increases. The linear fit of this dependence is

$$Mean(channel) = a_0 + a_1 * x(cm) \tag{6}$$

In the **Table 8** are presented the linear fit parameters for different DIRAC run periodes.

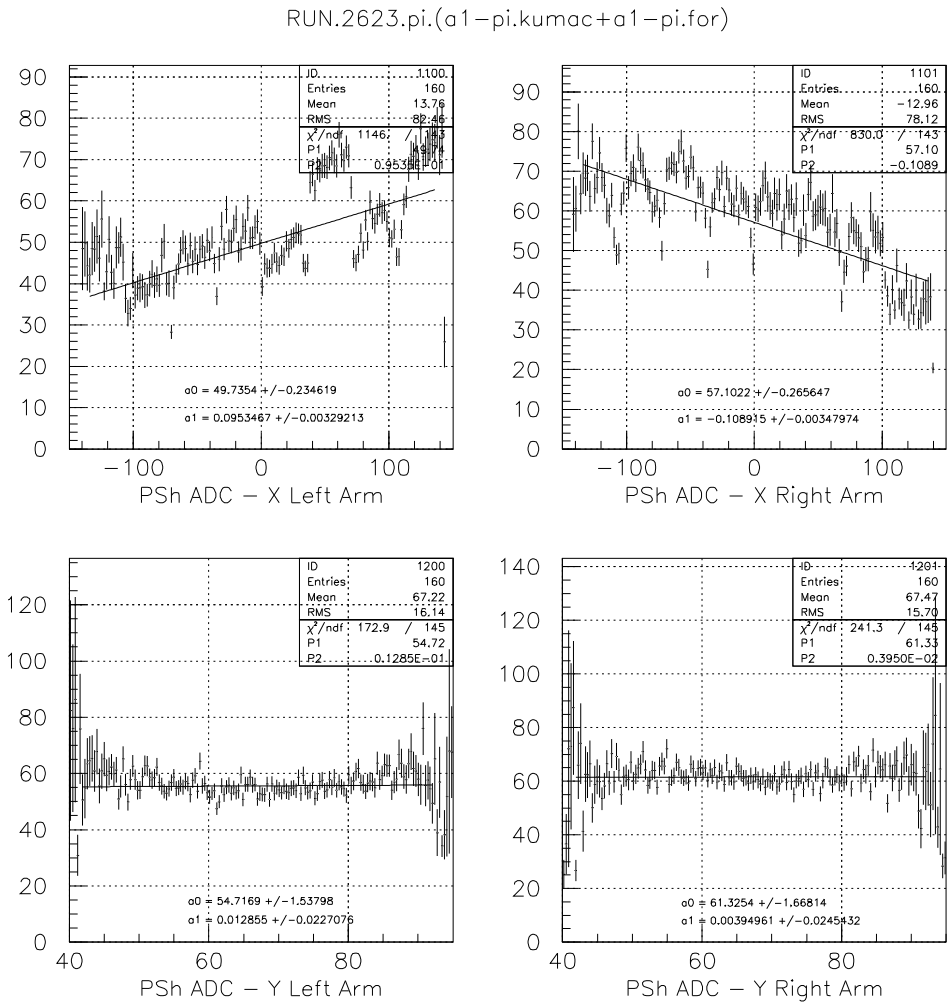

Figure 15: **Pion** amplitude (ADC channel) distribution versus x and y coordinates (cm)

Table 8.
Linear fit parameters of the Eq.(6) for x dependence of the **pion** mean amplitude (Fig. 15 up)

Run (Season Year)	Target	Left arm		Right arm	
		a_0 (chan)	a_1 (ch/cm)	a_0 (chan)	a_1 (ch/cm)
1454 (Autumn 1999)	Pt	84.43	0.23	101.45	-0.45
2061 (Summer 2000)	Ni	52.03	0.12	56.81	-0.12
2623 (Autumn 2000)	Ti	49.74	0.10	57.10	-0.11
2844 (Autumn 2000)	Ti	50.81	0.08	56.67	-0.08
3180 (Spring 2001)	Ti	56.22	0.16	63.72	-0.12
3665 (Summer 2001)	Ni	48.59	0.12	53.74	-0.11
4255 (Autumn 2001)	Ni	125.51	0.32	125.46	-0.26

Contrary to the electron case, the y dependence of the pion amplitude is practically absent (Fig. 15 down). This shows a good uniformity of the scintillator transmission light along y axis.

3.3 Particle x hit coordinate - momentum calibration

As a result of the particle momentum separation, the low momentum (1 - 2 GeV/c) particles are hitting the outermost PSh slabs, and the high momentum (5 - 6 GeV/c) particles hit the innermost PSh slabs of the DIRAC set-up. In Fig. 16 are presented the scatter-plot for momentum $p(MeV/c)$ dependence of the pion hit coordinate $x(cm)$, for the left arm, and in Fig. 17 is the analytical fit for the same dependence with the function:

$$x = \frac{A}{p} + B + C \cdot p \tag{7}$$

The local reference system has the x axis horizontally, along the PSh basis, originating in the center of the 8 slabs PSh panel, directed to the right side. The same dependence is for the right arm and also for electrons. In the **Table 9** are presented the fit parameters of Eq.(7) for $1300 < p < 6000\ MeV/c$ for different DIRAC run periodes.

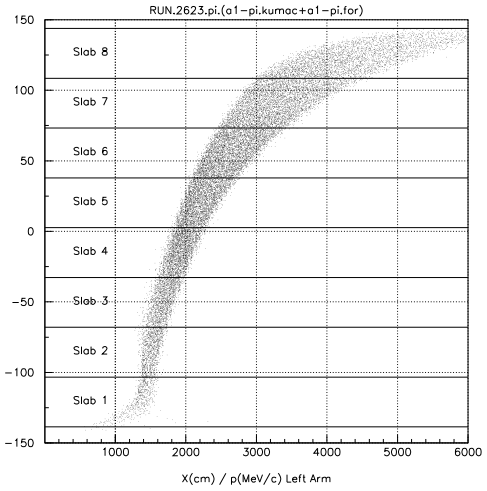

Figure 16: **Pion** x-coordinate hit (cm) versus momentum (MeV/c) scatter-plot of the PSh left arm

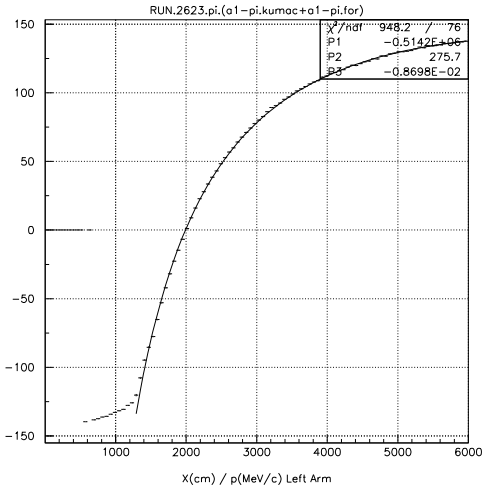

Figure 17: Fit of the x-coordinate hit (cm) versus momentum (MeV/c) dependence for **pion** signals in PSh left arm

Table 9.
The fit parameters of the Eq.(7) for momentum dependence of the **pion** x-coordinate hit (Fig. 17)

Run (Season Year)	Target	A (cm*MeV/c)	B (cm)	C (cm/MeV/c)
1454 (Autumn 1999)	Pt	-0.520E+06	280.2	-0.931E-02
2061 (Summer 2000)	Ni	-0.509E+06	273.4	-0.844E-02
2623 (Autumn 2000)	Ti	-0.514E+06	275.7	-0.870E-02
2844 (Autumn 2000)	Ti	-0.508E+06	270.7	-0.804E-02
3180 (Spring 2001)	Ti	-0.518E+06	278.5	-0.910E-02
3665 (Summer 2001)	Ni	-0.539E+06	293.2	-1.095E-02
4255 (Autumn 2001)	Ni	-0.532E+06	287.4	-1.011E-02

4 Multiple scattering effects on x and y hit distribution

We looked for the particle tracks, reconstructed from Drift Chamber data, incident on PSh detector. The PSh itself has been disconnected from the trigger scheme in this 1461 run. Nevertheless, the remaining trigger conditions ensure the same number of tracks (entries) both in the left and right arm.

The (x, y)-scatter plot of all incident tracks (hits) on PSh detector are presented in the first row of Fig. 18 (see also **Table 10**.). The corresponding x- and y-distributions are shown in the 2-nd row of Fig. 19 and Fig. 20.

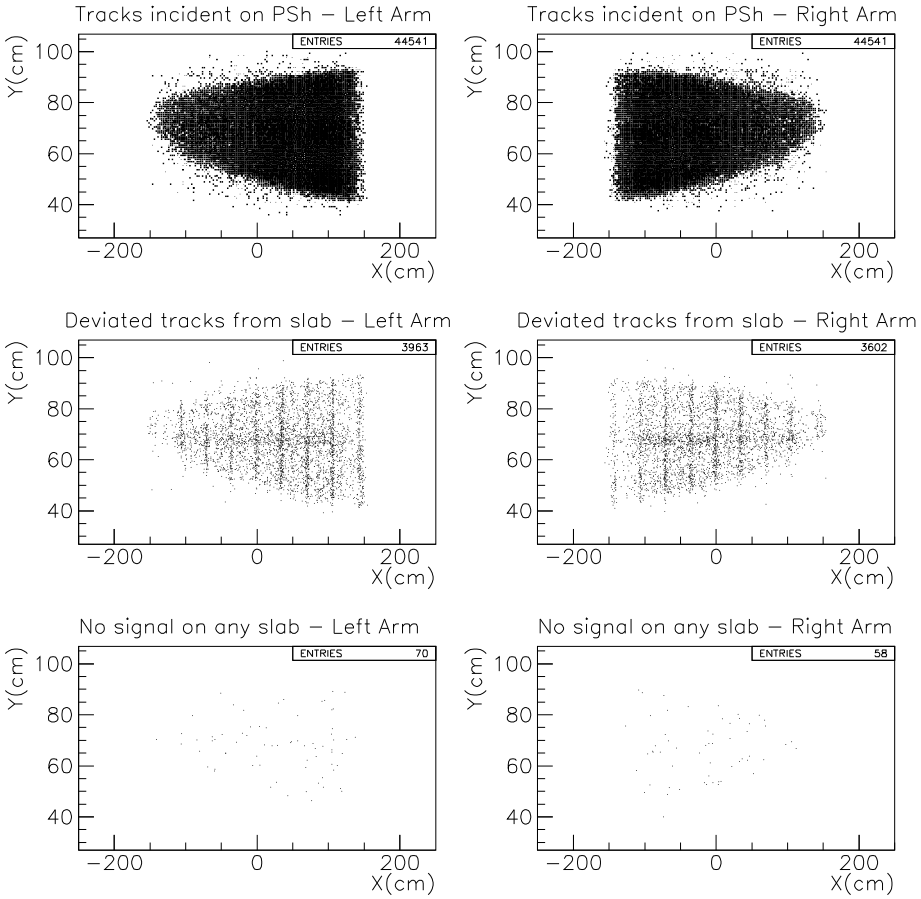

Figure 18: Reconstructed tracks incident on PSh detector

The detected tracks on the intersected slab (signals on hit slab) present the x- and y-distributions as shown in the 3-rd row Fig. 19 and Fig. 20 (see also **Table 10**).

The ratio detected/incident tracks on the specific slab measures PSh efficiency. The x- and y-distributions of the PSh efficiency are given in the first row of Fig. 19 and Fig. 20, as the ratios of the 3-rd and 2-nd row distributions.

Not all the tracks coming to PSh are detected with proper signals in the hit slab. Some of them are deviated by multiple scattering in the materials between Drift Chambers and PSh detector. They can be found either as signals in the neighbour slabs or out of the PSh detector. The (x, y)-scatter plot of the deviated tracks from the corresponding slab are shown in the 2-nd row Fig. 18 (see **Table 10** columns no.3 and no.6), and the x- and y-distributions are in the 4-th row Fig. 19 and Fig. 20. The x-distribution shows an enhancement of nondetected tracks in proper slab, along with slab boundary regions, as deviated tracks from the neighbour slabs. The y-distribution indicates also the existence of a scattering material before the PSh detector, in the median plane of the setup.

Table 10.

Preshower hit and signal statistics

Arm	Tracks incident on PSh	Tracks out of PSh	Tracks in PSh	Signals on hit slab	No signal on hit slab	No signal on hit slab but on other one	No signal on any slab
left	44541	245	44296	40578	3718	3648	70
right	44541	144	44397	40939	3458	3400	58

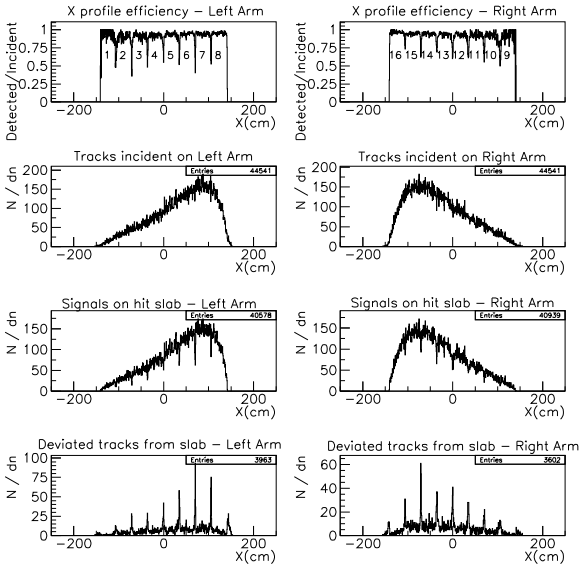

Figure 19: x profile track distributions

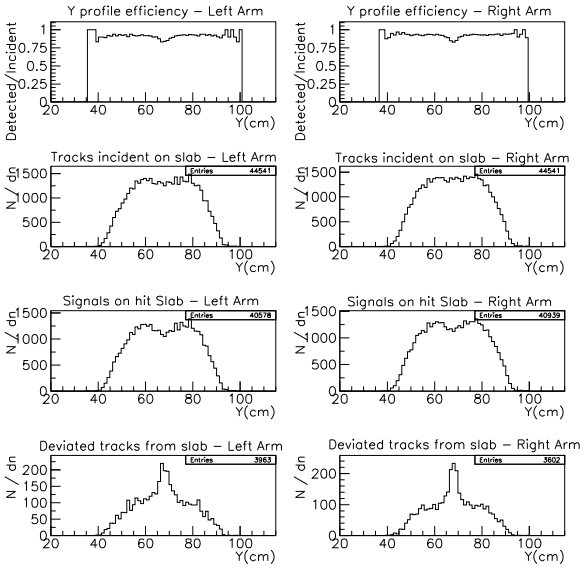

Figure 20: y profile track distributions

5 Conclusions

Has been analysed samples of "good pair events" during 1999 - 2001 DIRAC runs data taking in order to align PSh detector signals. The main results are:

1. Detector inhomogeneities for electron signals can be corrected slab by slab, using the fit parameters for electron peak position given in **Table 3**.
2. The mean electron and pion amplitude signals show a momentum dependence described by the fit parameters given in **Table 4** for electrons and in **Table 5** for pions.
3. Detector response dependence with the impact position of the particle show a linear x variation of the mean amplitude, both for electrons and for pions. It is directly connected with the x variation of the particle momentum (**Table 9**). The linear fit parameters for electron mean amplitude variation with x is presented in **Table 6** and the same dependence for pion mean amplitude is in **Table 8**
4. The y dependence of the amplitude signal for electrons is a more complicated one, with two quasi symmetrical parts, with a significant amplitude decrease in the central part of the detector. The slower decrease components were fitted by a linear dependence, with the fit parameters presented in the **Table 7**.
5. The y dependence of the pion signal is completely different. Practically it is independent on y, the signal has the same amplitude for all incident points along y axis of the detector.
6. The x - momentum calibration is given by the Eq.(7), with the fit parameters specified in **Table 9**.
7. The evaluation of the multiple scattering effect on position impact and x and y profile efficiency of the PSh detector is presented in **Table 10** and Figures 19 20.

References

[1] B. Adeva et al. - DIRAC Group, Proposal to the SPSLC, *Lifetime measurement of $\pi^+\pi^-$ atoms to test low energy QCD prediction*, CERN/SPSLC 95-1, SPSLC/P 284 (1995).

[2] H. Bozdog, Gh. Caragheorgheopol, M. Pentia, V. Zoran, S. Trusov, *Preshower Scintillation Detector for DIRAC Experiment* (experimental results), DIRAC Note 98-03, 25 Feb. 1998.

[3] M. Pentia, Gh. Caragheorgheopol, M. Ciobanu, D.Pop, C.Rusu, *Preshower Detector Commissioning along with DIRAC set-up*, DIRAC Note 99-03, 22 Feb. 1999.